

Lateral spin-orbit interaction and spin polarization in quantum point contacts

Anh T. Ngo,¹ Philippe Debray,² and Sergio E. Ulloa¹

¹*Department of Physics and Astronomy, and Nanoscale and Quantum Phenomena Institute, Ohio University, Athens, Ohio 45701-2979*

²*Department of Physics, University of Cincinnati, Cincinnati, Ohio, 45221*
(Dated: November 21, 2018)

We study ballistic transport through semiconductor quantum point contact systems under different confinement geometries and applied fields. In particular, we investigate how the *lateral* spin-orbit coupling, introduced by asymmetric lateral confinement potentials, affects the spin polarization of the current. We find that even in the absence of external magnetic fields, a variable *non-zero spin polarization* can be obtained by controlling the asymmetric shape of the confinement potential. These results suggest a new approach to produce spin polarized electron sources and we study the dependence of this phenomenon on structural parameters and applied magnetic fields. This asymmetry-induced polarization provides also a plausible explanation of our recent observations of a 0.5 conductance plateau (in units of $2e^2/h$) in quantum point contacts made on InAs quantum-well structures. Although our estimates of the required spin-orbit interaction strength in these systems do not support this explanation, they likely play a role in the effects enhanced by electron-electron interactions.

PACS numbers: 71.70.Ej, 73.23.Ad, 72.25.-b, 72.10.-d

I. INTRODUCTION

The possibility of exploiting the spin degree of freedom of charge carriers in novel electronic devices is a tantalizing goal and an area of research attracting much interest recently.¹ Many of the devices studied consider low-temperature ballistic transport through quantum point contacts (QPCs). QPCs are typically formed in semiconductor heterostructures by defining “split” metal top gates. Via the application of voltages this split gate can create a short quasi-one-dimensional channel which separates two regions of two-dimensional electron gas (2DEG) lying near the heterojunction. This relatively simple nanoscale structure exhibits quantized conductance plateaus in units of $2e^2/h$, as function of gate voltage, as the effective QPC width increases with voltage. This behavior can be understood in terms of the quasi-1D channel being an electronic wave guide, allowing carriers to pass in successive transversely quantized channels.^{2,3,4} Other approaches for creating a QPC include direct etching of the material, or alternatively by the suitable oxidation of a surface layer, allowing in either case the creation of lateral in-plane gates.⁵ QPCs have been widely used in a variety of geometries and experiments, such as magnetic focusing, edge states in quantum Hall systems, as well as in transport through quantum dots.^{4,6}

When considering electronic transport in semiconductors, it has now become clear that it is essential to take into account the impact that the spin-orbit (SO) interaction has on the dynamics of carriers and especially on their spin.⁷ This relativistic effect is sizable and ubiquitous in these systems, although the strength of the SO coupling depends on the host materials used, as well as sensitively on the confinement fields, via the Rashba mechanism.⁸ Studies of transport properties of a 2DEG in the presence of SO interactions under different confine-

ment potentials have been reported in the literature,^{7,9} including QPC structures.^{10,11} The general symmetry properties of spin-dependent conduction coefficients in two terminal measurement setups have also been discussed recently.¹² These studies show that SO interactions may give rise to interesting electric-field generated spin-polarization along the plane of the 2DEG.^{10,11}

The theoretical work presented here is motivated by recent experiments at the University of Cincinnati,¹³ which exhibit unique conductance quantization in side-gated QPCs made on InGaAs/InAs heterostructures. These experiments demonstrate that QPCs with asymmetric lateral confinement show “half” quantized plateaus ($\simeq 0.5 \times 2e^2/h$), suggestive of full spin-polarized conduction. As the InAs host material exhibits strong SO coefficients (having a smaller energy gap than GaAs, for example), a natural possibility for this behavior is that a polarization develops due to the strong SO effect. This paper is devoted to analyze this possibility, as well as to explore in general the importance of *lateral* fields on the observed conductance of the QPC. Using a scattering matrix approach,^{12,14} we study ballistic transport through semiconductor QPCs under different confinement geometries and external fields. In particular, we investigate how the SO coupling induced by a lateral confinement potential, arising from the side-gates in the system, may result in spin polarization of the current. We find that for suitably laterally asymmetric QPC geometries (and corresponding asymmetric lateral electric fields) and strong SO coupling constants, it is indeed possible to observe spin-polarized transport coefficients, *even in the absence of magnetic fields*. A high spin polarization is in principle possible, and consistent with the general symmetry properties of two-terminal systems.¹² We analyze the conditions under which this polarization may take place and compare with the known and estimated parameters

of the structure used in experiments.¹³ Our results in general provide a possible new mechanism to implement spin-polarized electron sources on realistic materials and structure parameters. Large polarization is also possible for stronger SO coupling constants (narrower gap), such as InSb, as we will discuss in detail.¹⁵

In what follows, we introduce the model for QPCs, as well as the computational approach to calculate transport coefficients in Sec. II. Results for different structures and applied fields are presented in Sec. III, together with a discussion of their physical significance in experiments, especially those of Ref. [13].

II. THEORETICAL MODEL

We consider a two-dimensional electron gas (2DEG) confined to a plane perpendicular to the z -axis. The confining electric field in the z direction (coming from the heterostructure band alignments, as well as doping profiles and applied top gate potentials in general) results in the “usual” Rashba SO interaction,⁸

$$H_{SO}^R = \frac{\alpha}{\hbar}(\sigma_x P_y - \sigma_y P_x), \quad (1)$$

where σ_x and σ_y are Pauli matrices, P_x and P_y denote the kinetic momentum, and α is the Rashba SO coupling. The electronic transport of interest occurs through a QPC defined on the 2DEG via the confining potential $V(x, y) = U(x) + V_a(x, y)$, where $U(x)$ describes a hard wall potential ($U(x) = 0$ for $0 \leq x \leq W$, and $U = \infty$ otherwise), arising from the etching process in our system and which therefore defines the overall channel structure. The $V_a(x, y)$ potential can be thought to arise from the lateral gates in the system, and as such it defines the QPC’s symmetry. We adopt a simple function, used recently to describe QPCs,¹⁰ to write

$$V_a(x, y) = \frac{V_g}{2} \left(1 + \cos \frac{\pi y}{L_y} \right) + \frac{1}{2} m^* \omega^2 x_-^2 \Theta(x_-), \quad (2)$$

with $x_- = x - x_a$, and

$$x_a = W_0 \left(1 - \cos \frac{\pi y}{L_y} \right). \quad (3)$$

Here, $\Theta(x)$ is the step function, m^* is the effective mass of the electron, L_y is the characteristic size of the structure in the y -direction, $W_0 (< W)$ is a constant, and ω is the frequency of the parabolic confinement potential. Notice that this potential form is asymmetric in the x direction and its amplitude is controlled by the gate potential V_g , as well as by ω . See Fig. 1b for a typical asymmetric QPC potential profile structure. Correspondingly, the asymmetric confinement field gives rise to a *lateral* SO interaction which further couples the spin and orbital degrees of freedom.¹⁶ This lateral SO potential takes the form⁷

$$V_{SO}^\beta = -\frac{\beta}{\hbar} \nabla \mathbf{V} \cdot (\hat{\sigma} \times \hat{\mathbf{P}}), \quad (4)$$

where $\beta = \hbar^2/4m^*c^2$. The total Hamiltonian of the QPC system is then given by

$$H = \frac{P_x^2 + P_y^2}{2m^*} + H_{SO}^R + V(x, y) + V_{SO}^\beta. \quad (5)$$

We will also consider the case of *symmetric* QPCs, in order to contrast their behavior with the asymmetric potential profiles. We model the symmetric QPC with a confinement potential given by

$$V_s(x, y) = \frac{V_g}{2} \left(1 + \cos \frac{\pi y}{L_y} \right) + \frac{1}{2} m^* \omega^2 (x - x_s)^2 \times \Theta(\pm(x - x_s)), \quad (6)$$

with

$$x_s = \frac{W}{4} \left(1 - \cos \frac{\pi y}{L_y} \right). \quad (7)$$

Notice that as the potential profile is symmetric in the x direction, there is no net contribution from the lateral SO interaction to the resulting dynamics, and this fact will be reflected in its transport coefficients, as we will show below. We should mention that this QPC profile is similar to that used by Eto *et al.*,¹⁰ and is depicted in the top panel of Fig. 2.

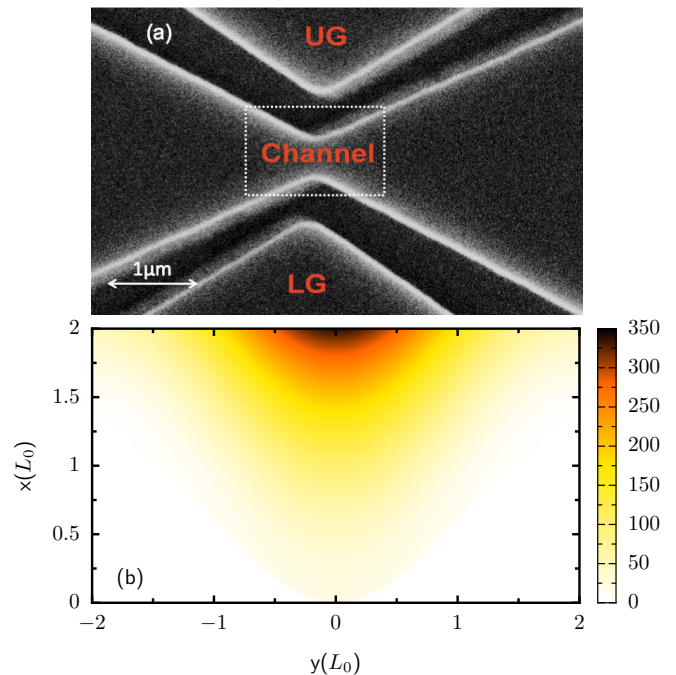


FIG. 1: (Color online) (a) Scanning micrograph of typical InAs QPC¹³. The upper (UG) and lower (LG) gates are separated from the active channel by v-shaped etch trenches. The QPC potential profile for the region in the dashed box is schematically shown in lower panel. (b) Strongly asymmetric potential profile as in Eq. (2), for $V_g = 20E_0$, $W_0 = 0.6L_0$ and $L_y = 2L_0$, includes hard walls at $x = 0$ and $x = W = 2L_0$. E_0 and L_0 are energy and length units defined in text.

In order to calculate the transport coefficients through the QPC system (either symmetric or asymmetric), we use a wonderful scattering-matrix formalism developed to study spin-dependent electron transport in two-terminal geometries.¹⁴ For ease of calculation, the SO coupling α and $V(x, y)$ are set to zero at the source and drain reservoirs, but are turned on at the lead-sample interface (for $|y| \leq L_y$). The solution of the Schrödinger equation in the leads is represented by a set of transverse eigenvectors $|n\rangle$ and eigenvalues ϵ_n , so that the electron wave function in the leads can be written in the form $e^{ik_y y} |n\sigma\rangle$, with $\sigma = \uparrow$ or \downarrow representing the spin-up or spin-down state. We further decompose the confinement potential into N narrow strips along the y -direction, so that in strip i the potential $V(x, y)$ is y -independent, $V(x, y_i) = V_c(x)$, and $V_{SO}^\beta = -\frac{\beta}{\hbar} \left(P_y \frac{d}{dx} V_c(x) - P_x \frac{d}{dy} V|_{y=y_i} \right) \sigma_z$. The electron eigenvectors in each strip j can then be described in terms of the wave functions in the leads,

$$|\Psi\rangle_j = \sum_{n\sigma} a_n^\sigma |n\sigma\rangle e^{ik_y^j y}. \quad (8)$$

Utilizing this formulation, the Schrödinger equation defined by the Hamiltonian, Eq. (5), results in the matrix equation:

$$\begin{pmatrix} \mathbf{0} & \mathbf{1} \\ \mathbf{S} & \mathbf{T} \end{pmatrix} \begin{pmatrix} \mathbf{D} \\ \mathbf{F} \end{pmatrix} = k_\gamma \begin{pmatrix} \mathbf{D} \\ \mathbf{F} \end{pmatrix}, \quad (9)$$

where $(\mathbf{S})^{\sigma\sigma'}$ contains $(E - \epsilon_n)\delta_{mn}^{\sigma\sigma'}$ and the matrix elements of $\langle m|V_c(y)|n\rangle$ and $\langle m|V_{SO}^\beta|n\rangle$, while

$$(\mathbf{T})_{mn}^{\sigma\sigma'} = -\alpha\delta_{mn}^{\sigma\sigma'}, (\mathbf{F})_{n\gamma}^\sigma = k_\gamma a_{n\gamma}^\sigma, (\mathbf{D})_{n\gamma}^\sigma = a_{n\gamma}^\sigma, \quad (10)$$

following Ref. [14].

For a given incident energy E , Eq. (9) gives a set of wave numbers, k_γ , and set of corresponding eigenvectors, $a_{n\gamma}^\sigma$ within each strip. The set of wave numbers is divided into two groups, the first consisting of $k_{I\gamma}$, which are complex but have a positive imaginary part, or those which are real and have a positive mean velocity. The second group consists of wave numbers $k_{II\gamma}$, which are complex and have a negative imaginary part, or which are real and have a negative mean velocity. The wave function in the stripe j is then written as

$$|\Psi\rangle_j = \sum_{\gamma n\sigma} [a_{I\gamma}^{(j)\sigma} b_{I\gamma}^j e^{ik_{I\gamma}^j (y-y_0^j)} + a_{II\gamma}^{(j)\sigma} b_{II\gamma}^j e^{ik_{II\gamma}^j (y-y_0^j)}] |n\sigma\rangle. \quad (11)$$

Here y_0^j is the reference coordinate for the strip j at the interface with strip $j+1$. The continuity requirements on the electron probability density and flux density, i.e., $\Psi^j|_{y=y_0^{j+1}} = \Psi^{j+1}|_{y=y_0^{j+1}}$ and $\hat{v}_y^j \Psi^j|_{y=y_0^{j+1}} = \hat{v}_y^{j+1} \Psi^{j+1}|_{y=y_0^{j+1}}$, where $\hat{v}_y = \frac{i}{\hbar} [H, y]$ is the velocity operator in the y direction, lead to a set of linear equations relating the wave function expansion coefficients in neighboring strips j and $j+1$:

$$\begin{pmatrix} \mathbf{B}_I^j \\ \mathbf{B}_{II}^j \end{pmatrix} = \mathbf{M}(j, j+1) \begin{pmatrix} \mathbf{B}_I^{j+1} \\ \mathbf{B}_{II}^{j+1} \end{pmatrix}, \quad (12)$$

where \mathbf{B}_I^j and \mathbf{B}_{II}^j are vectors containing coefficients $\{b_{I\gamma}^j\}$ and $\{b_{II\gamma}^j\}$, respectively, and $\mathbf{M}(j, j+1)$ is the transfer matrix between contiguous strips. The full transfer matrix for the structure, $\mathbf{M}(L, R)$, relating the coefficients in the left and right leads is found from the matrix product of the individual matrices connecting strips. This formulation, however, is known to exhibit numerical instabilities especially in large systems. By defining a scattering matrix $\mathbf{S}(L, R)$, relating the outgoing waves from the sample to those incoming into the QPC, one can remove the numerical instabilities to a great extent.¹⁴ The system of linear equations then becomes:

$$\begin{pmatrix} \mathbf{B}_I^R \\ \mathbf{B}_{II}^R \end{pmatrix} = \mathbf{S}(L, R) \begin{pmatrix} \mathbf{B}_I^L \\ \mathbf{B}_{II}^L \end{pmatrix}, \quad (13)$$

where the elements of the scattering matrix \mathbf{S} are given in terms of those of the transfer matrix \mathbf{M} .¹⁴

The transport coefficients are obtained after imposing the incident-from-the-left boundary condition on the electron wave function as $\mathbf{B}_{II}^R = 0$ and $\mathbf{B}_I^L = \mathbf{I}_m^{\sigma'}$ for left-lead channel m with spin σ' , where $\mathbf{I}_m^{\sigma'}$ is a unit vector. This results in

$$\begin{aligned} \mathbf{B}_I^R &= \mathbf{S}_{11}(L, R) \mathbf{I}_m^{\sigma'}, \\ \mathbf{B}_{II}^L &= \mathbf{S}_{21}(L, R) \mathbf{I}_m^{\sigma'}. \end{aligned} \quad (14)$$

The linear conductance of the system at finite temperature T is then given by

$$\begin{aligned} G(T) &= \frac{e^2}{h} \int_0^\infty \sum_{r, n\sigma m\sigma'}^r t_{nm}^{\sigma\sigma'}(E) \left(-\frac{\partial f(E, T)}{\partial E} \right) dE \\ &= G^{\uparrow\uparrow}(T) + G^{\uparrow\downarrow}(T) + G^{\downarrow\uparrow}(T) + G^{\downarrow\downarrow}(T), \end{aligned} \quad (15)$$

where $t_{nm}^{\sigma\sigma'} = k_n^\sigma |b_{In}^\sigma|^2 / k_m^{\sigma'}$ is the transmission coefficient from channel m and spin σ' to channel n and spin σ , $f(E, T)$ is the Fermi-Dirac distribution function, and the r superindex in the summation symbol indicates that the sum is taken over all states that have k_n^σ real. For spin-dependent conductances it is useful to calculate the spin polarization:

$$P = \frac{G^\uparrow - G^\downarrow}{G^\uparrow + G^\downarrow} = \frac{G^{\uparrow\uparrow} + G^{\uparrow\downarrow} - G^{\downarrow\uparrow} - G^{\downarrow\downarrow}}{G}, \quad (16)$$

which gives a measure of current polarization in the system.

III. RESULTS AND DISCUSSION

We present results for a QPC fabricated on InAs, as in the experiment,¹³ with effective mass $m^* = 0.023m_0$, g-factor $g = 14$ (see Ref. 17) and take typical values of length and energy to normalize the different quantities, $L_0 = \sqrt{\hbar/m^*\omega_0} = 32.5$ nm, $E_0 = \hbar^2/m^*L_0^2 = 3.12$ meV, with $\omega_0 = 4.74 \times 10^{12} \text{s}^{-1}$, and $\alpha_0 = E_0 L_0 = 10.1 \times 10^{-11}$ eV m representing typical spin-orbit coupling

strength. The width of hard wall confining potential is set to $W = 2L_0$, while the confinement frequency in Eq. (2) is kept constant and chosen relatively large, $\omega = 12.6\omega_0$, as well as a strong coupling $\beta = 0.97 \times 10^{-16} \text{ m}^2$ (values used throughout, unless stated otherwise).

To illustrate the well-known conductance quantization of a QPC but now in the presence of SO interactions, Fig. 2b shows the spin-dependent conductances for the *symmetric* QPC system shown in the top panel. The conductances are shown as function of V_g for given Fermi energy, $E_F = 48E_0$, and moderate SO strength, $\alpha = 0.25\alpha_0$ (notice that since there is no net contribution of the lateral SO effect, the value of β is irrelevant). The total conductance is clearly quantized, as expected, with each of the spin channels contributing equally. Notice that as the QPC includes a Rashba SO term, the different $G^{\sigma\sigma'}$ partial spin conductances exhibit an oscillatory behavior with SO coupling strength α , similar to the well-known Datta-Das response,¹⁸ as seen in Fig. 2c for the first conductance plateau at $V_g = 35E_0$. We stress that despite variations in the partial conductances, the spin-polarization of the symmetric QPC is *always null*. We should comment that these results are anticipated from the general symmetry properties discussed by Zhai and Xu,¹² as the confining potential and Rashba SO interaction are symmetric under reflection, $V(x, y) = V(-x, y)$ and $\alpha(x, y) = \alpha(-x, y)$. In contrast, as we will see below, the lateral SO interaction in an asymmetric QPC results in non-zero spin polarization.

In the case of the *asymmetric* confinement potential of Fig. 1b, the conductance is shown in Fig. 3a as function of the gate potential V_g , which controls the height of the barrier in the QPC at $y = 0$, and therefore the opening of the QPC, and to some degree also its asymmetry. The arrows \uparrow and \downarrow label the curves for spin-up and -down conductances, respectively. This figure assumes a moderate SO strength $\alpha = 0.25\alpha_0$ and Fermi energy $E_F = 48E_0$. For these realistic parameter values, similar to those in Fig. 2, we see that the total conductance is appropriately quantized in units of $2e^2/h$, while there is also a small but non-zero spin polarization, especially near the transition to the second plateau, as shown explicitly in Fig. 3b. This illustrates one of our main results, that *in the absence of external magnetic field and unpolarized injection*, it is possible to have spin-polarization in a strongly *asymmetric* QPC, as that depicted in Fig. 1b. This is in contrast to the null spin polarization in symmetric QPCs, showing that the asymmetric electric field introduced by the lateral SO interaction is essential for the appearance of polarization, in accordance with general symmetry considerations.¹² A gradually appearing asymmetry, which can be easily implemented in the potential of Eq. (2), gives rise to increasing polarization, as one would anticipate (not shown).

The finite polarization for asymmetric potentials in the presence of lateral SO interactions can be traced back to the details of the resulting channel (sub-band) dispersion curves, as the lateral SO introduces channel mixtures or

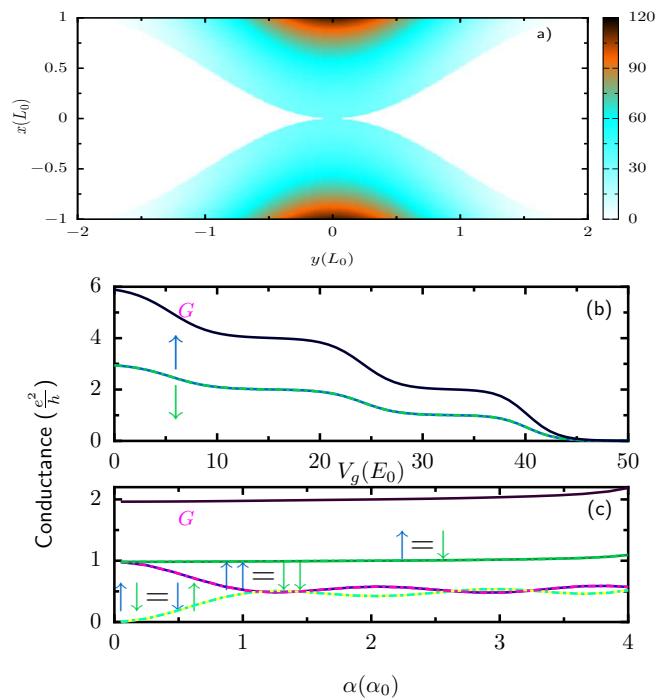


FIG. 2: (Color online) (a) Symmetric QPC potential profile for $V_g = 35E_0$ in Eq. (7). (b) Spin-dependent conductances vs. V_g for fixed Fermi energy $E_F = 48E_0$ and $\alpha = 0.25\alpha_0$. Notice quantized plateaus as QPC opens for decreasing V_g . (c) At the first conductance plateau, $V_g = 35E_0$, the partial conductances $G^{\sigma\sigma'}$ exhibit oscillations with coupling strength α . Notice there is no spin polarization in this confinement geometry even for large SO coupling.

anti-crossing features.^{10,19} The avoided crossings in the subband structure effectively generate spin rotations as electrons pass the narrow constriction of the QPC. This structure is drastically modified in the absence of lateral SO interaction. Notice that results presented here differ with previous work reporting spin-polarization across QPCs,^{10,11} on two important points: (a) we consider here z -axis polarization – unlike the *in-plane* spin polarization considered previously (in other words, spin-up and -down electrons refers to the y -axis quantization direction in those cases); (b) most essential is that we consider an asymmetric lateral confinement potential, giving rise to non-zero *lateral* SO interaction.

In order to study the interplay between the SO interaction in the different directions (Rashba vs. lateral SO), Fig. 4a shows spin-dependent conductances and the conductance polarization as function of Rashba coupling α (which could perhaps be varied via the application of different voltages to a top gate covering the entire structure, for example). These results are calculated at $V_g = 20E_0$, corresponding to the first conductance plateau (see Fig. 3a) in the asymmetric QPC in Fig. 1b. We see that conductances G_\uparrow and G_\downarrow are very different from each other, and oscillate widely with varying α . G_\uparrow values larger than e^2/h are accompanied by a drop in G_\downarrow over

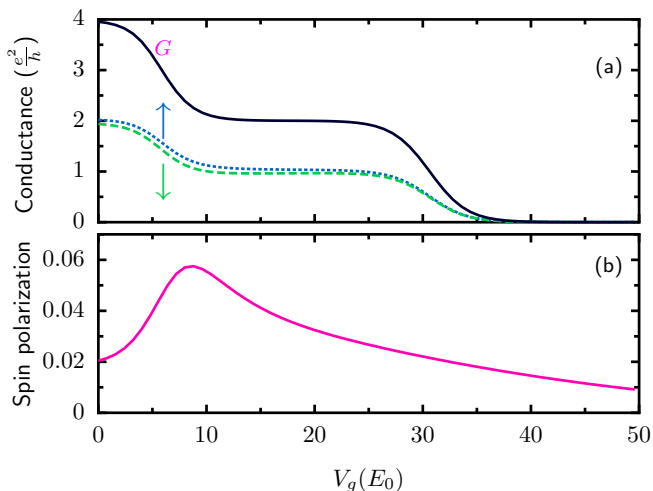


FIG. 3: (Color online) Results for *asymmetric* QPC potential profile as in Fig. 1b. Spin-dependent conductance (a) and polarization (b) as function of gate voltage V_g at fixed Fermi energy $E = 48E_0$. Arrows \uparrow and \downarrow indicate the results for spin up and spin down conductances, respectively. Parameters used are $\omega = 12.6\omega_0$, $\alpha = 0.25\alpha_0$, $W_0 = 0.6L_0$, $W = 2L_0$, and $L_0 = 32.5$ nm.

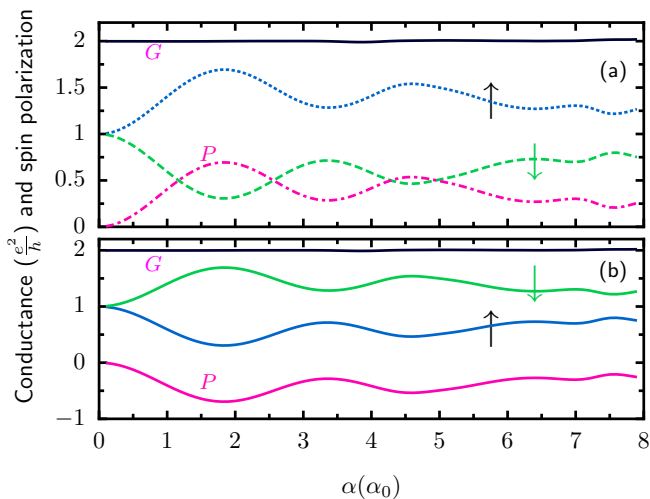


FIG. 4: (Color online) Conductance and spin polarization as function of Rashba SO coupling α for an asymmetric QPC. Structure parameters as in Fig. 3 at $V_g = 20E_0$. All partial spin-conductance curves oscillate with α , as expected for a multi-channel Datta-Das system, while the total conductance remains constant. (a) Results for QPC with potential profile as in Fig. 1b. (b) Results for *reversed* potential profile, $V \rightarrow V(-x, y)$ with respect to that in (a). Non-zero polarization direction is reversed for reversed profile.

the same range, indicating that a strong spin rotation takes place in the QPC region (even as the total conductance remains quantized at $2e^2/h$). The strong SO interaction induced by the Rashba field is able to mix different channel subbands in the QPC region, so that a large G_\uparrow ($> e^2/h$) is possible. In this range of large spin

rotation, the conductance polarization can reach nearly 70% (for $\alpha \approx 1.8\alpha_0$). It is also interesting to verify that the polarization axis is determined by the asymmetry in the QPC confinement potential and the lateral SO. To demonstrate this effect, we have calculated the conductance for a QPC with a “reversed” confining potential, so that the in-plane field giving rise to the lateral SO reverses direction. As shown in Fig. 4b, we find that the partial up/down spin conductance curves are exchanged, so that the resulting polarization reverses sign. This interesting behavior could in principle allow one to control the spin polarization of the device by changing the asymmetry of the lateral confining potential.

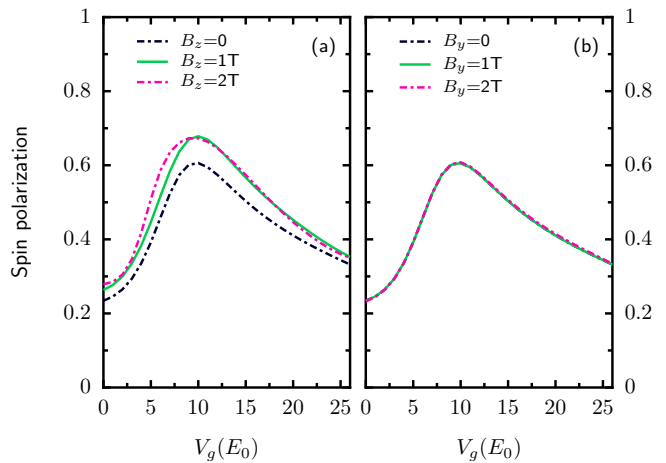


FIG. 5: (Color online) Conductance polarization for asymmetric QPC as function of V_g for given Fermi energy, $E_F = 48E_0$ and $\alpha = 1.0\alpha_0$. (a) Results for perpendicular magnetic field, $B_z = 0, 1$ and $2T$, show strong variation with field value. (b) Polarization for in-plane fields, parallel to the current direction, show large values due to asymmetry, but nearly field-independence; shown here for $B_y = 0, 1$ and $2T$.

Let us now analyze the effect of applied magnetic field in two different directions, perpendicular to the 2DEG—along the z axis, which couples to the spins and orbital motions of the electrons—and an in-plane field, which couples only to the spins via the Zeeman effect. Both directions of magnetic field result in a Zeeman term $g\mu_B\vec{\sigma} \cdot \vec{B}$, while a perpendicular field introduces an additional effective dynamical confinement. This arises from the replacement of the momentum by $\vec{P} - e/c\vec{A}$, where $\vec{A} = (-B_z y, 0, 0)$ is the vector potential associated with B_z . The presence of a field in the z -direction results in an anticipated conductance polarization, even for low QPC asymmetries and weak fields. Moreover, the magnetic field enhances the overall polarization, as seen in Fig. 5a. In contrast, an in-plane magnetic field along the y -axis (parallel to the current direction) does not significantly change the conductance polarization curves; this insensitivity to the presence of the B_y field is shown in Fig. 5b. We should stress that setting the SO couplings to zero results in nearly null polarization, even in the presence

of the magnetic fields shown (a high field does produce polarization by itself). We also find that the polarizing nature of the QPC is dominated by the lateral SO interactions (as one can easily verify if $\alpha = 0$, for example—not shown). It would be interesting to be able to probe the different polarization and its sensitivity to lateral SO effects in experiments which can vary field direction and can directly assess the polarization of the conductance.²⁰

As discussed in the introduction, a major motivation for the study we present here was the observation of $\simeq 0.5$ conductance plateaus (in units of $2e^2/h$, Fig. 6a) seen in asymmetric QPCs created on structures as that shown in Fig. 1a. A natural explanation of this observation, considering the theoretical results we have just discussed above, would be to assume that the QPCs on InAs hosts with asymmetric lateral confinement used in Ref. 13 have relatively large values of the SO coupling constants. This unique situation would be further aided by the in-plane gate techniques which allow the realization of asymmetric confinement potentials giving rise to the lateral SO (via asymmetric voltages on the UG and LG gates). We have demonstrated, as exemplified above, that variation of the α SO coupling constant, as well as variation of the asymmetry in the QPC (via our V_g and ω parameters) is able to produce strong conductance polarization (for non-zero β lateral SO coupling). However, extensive exploration of variations of these parameters over reasonable ranges (in accordance with experimental estimates for physically appropriate values) is *not able* to produce the 0.5 plateaus. We therefore conclude that the source of this strong polarization lies beyond the single-particle Hamiltonian studied here, and that possible electron-electron interaction effects may be responsible for the observed behavior. Detailed discussions of those effects are found in recent work by our collaborators.^{13,21}

Although the nature of electron-electron interaction and its role in producing 0.5 conductance plateaus is rather subtle (and beyond the purview of our work here), one can characterize their effect when compared with our single-particle Hamiltonian. One simple way to achieve 0.5 plateaus in this context is to consider an effective *ad hoc* perpendicular magnetic field that only breaks the up/down spin symmetry (and yet is assumed to not couple to the charge dynamics). Correspondingly, we add an effective Zeeman term to the single-particle Hamiltonian, Eq. (5), of the form $\Delta_0 f(y)\sigma_z$, where $f(y)$ is a smooth function that is 1 inside the QPC and gradually decreases to zero in the leads [we take $f(y) = \cos^2(\pi y/12L_0)$ for $-6 \leq y/L_0 \leq -2$ and $2 \leq y/L_0 \leq 6$, while $f(y) = 1$ for $|y/L_0| \leq 2$], and Δ_0 is a strength parameter. This term clearly breaks time reversal symmetry and produces a 0.5 plateau structure in the total conductance of the QPC system for large enough Δ_0 . Figure 6b shows a clear 0.5 plateau, qualitatively similar to that seen in experiments. We should point out that these curves include the lateral SO but do not include a Rashba term, since the absence of a top gate in the experiments with samples on nominally symmetric quantum wells, results in a small value of

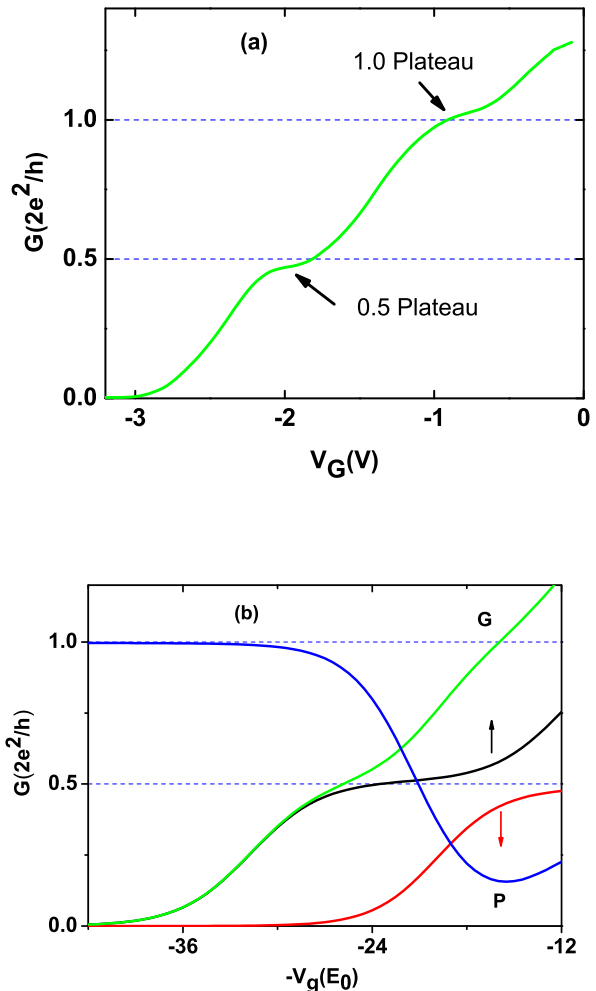


FIG. 6: (Color online) (a) Experimental conductance of QPC measured at an asymmetry of 7.5 V between UG and LG gates,¹³ showing clear 0.5 plateau in the absence of applied magnetic fields. (b) Theoretical results for conductance and spin polarization with *ad hoc* z -field chosen to produce a 0.5 plateau structure. Structural parameters used here are as in experiments $L_0 = 30\text{nm}$, $E_0 = 3.67\text{ meV}$, $\alpha = 0$, $\beta = 1.8 \times 10^{-18}\text{ m}^2$,¹³ while $\Delta_0 = 6E_0$ (see text).

$\alpha \simeq \text{const}$ throughout the QPC (and assumed zero). The calculations yield a 0.5 plateau, as expected, but require a strong z -axis spin-polarizing field, $\Delta_0 \geq 5E_0$ ($\simeq 22\text{ T}$ for $g = 14$ in InAs¹⁷), for the plateau to be well-defined.

In summary we have studied the competition between Rashba and lateral spin-orbit terms in the Hamiltonian of ballistic electrons moving through semiconductor quantum point contact systems of different confinement geometries and under different applied magnetic fields. We have shown that the lateral spin-orbit coupling, as induced by laterally-asymmetric confinement potentials results in non-vanishing spin polarization of the current

through the quantum point contact. Our numerical results are consistent with the general symmetry properties of two-terminal transport coefficients. We find that in the absence of external magnetic fields, it is possible to obtain high spin polarization and control its direction, by tailoring the asymmetry of the lateral confinement potential. Further application of magnetic fields results in stronger polarization, as one would expect (although larger than for the magnetic field alone). We believe that physically reasonable values of the different coupling constants and structural features can result in strong polarization in realistic systems. This would allow one to produce polarized currents in an all-electric con-

figuration, a desirable goal for spintronic applications.¹³ Finally, although fascinating experimental results show full polarization of the conductance in strongly asymmetric quantum point contacts, the calculations we present here cannot explain those observations for experimental estimates of the different structure parameters. It is then presumed that electron-electron interactions must play an essential role in these observations, as discussed elsewhere in the literature.^{13,21}

The authors acknowledge support of CMSS and BNNT programs at Ohio University, as well as NSF grants 0710581 and 0730257 (Ohio), and NSF ECCS 0725404 (Cincinnati).

-
- ¹ S. A. Wolf, D. D. Awschalom, R. A. Buhrman, J. M. Daughton, S. von Molnár, M. L. Roukes, A. Y. Chtchelkanova, D. M. Treger, *Science* **294**, 1488 (2001).
- ² B. J. van Wees, H. van Houten, C. W. J. Beenakker, J. G. Williamson, L. P. Kouwenhoven, D. van der Marel and C. T. Foxon, *Phys. Rev. Lett.* **60**, 848 (1988).
- ³ D. A. Wharam, T. J. Thornton, R. Newbury, M. Pepper, H. Ahmed, J. E. F. Frost, D. G. Hasko, D. C. Peacock, D. A. Ritchie and G. A. C. Jones, *J. Phys. C: Solid State Phys.* **21** L209 (1988).
- ⁴ C. W. J. Beenakker and H. van Houten, *Solid State Phys.* **44**, 1 (1991).
- ⁵ See for example, S. Luscher, A. Fuhrer, R. Held, T. Heinzel, K. Ensslin, and W. Wegscheider, *Appl. Phys. Lett.* **75**, 2452 (1999).
- ⁶ R. Hanson, L. P. Kouwenhoven, J. R. Petta, S. Tarucha, and L. M. Vandersypen, *Rev. Mod. Phys.* **79**, 1217 (2007).
- ⁷ R. Winkler, *Spin-Orbit Coupling Effects in Two Dimensional Electron and Hole Systems* (Springer, Berlin, 2003).
- ⁸ Y. A. Bychkov and E. I. Rashba, *J. Phys. C* **17**, 6039 (1984).
- ⁹ A. T. Ngo, J. M. Villas-Bôas, and S. E. Ulloa, *Phys. Rev. B* **78**, 245310 (2008).
- ¹⁰ M. Eto, T. Hayashi, and Y. Kurotani, *J. Phys. Soc. Japan.* **74**, 1934 (2005).
- ¹¹ A. Reynoso, G. Usaj, and C. A. Balseiro, *Phys. Rev. B* **75**, 085321 (2007).
- ¹² F. Zhai and H. Q. Xu *Phys. Rev. Lett.* **94**, 246601 (2005).
- ¹³ P. Debray, S. M. S. Rahman, J. Wan, R. S. Newrock, M. Cahay, A. T. Ngo, S. E. Ulloa, S. T. Herbert, M. Muhammad, and M. Johnson, *Nature Nanotech.*, in press (2009).
- ¹⁴ L. Zhang, P. Brusheim, and H. Q. Xu, *Phys. Rev. B* **72**, 045347 (2005).
- ¹⁵ See for example, C. F. Destefani, S. E. Ulloa, and G. E. Marques, *Phys. Rev. B* **70**, 205315 (2004); H. Chen, J. J. Heremans, J. A. Peters, J. P. Dulka, A. O. Govorov, N. Goel, S. J. Chung, and M. B. Santos, *Appl. Phys. Lett.* **86**, 032113 (2005).
- ¹⁶ Y. Jiang and L. Hu, *Phys. Rev. B* **74**, 075302 (2006); Y. Xing, Q.-F. Sun, L. Tang, and J. P. Hu, *Phys. Rev. B* **74**, 155313 (2006).
- ¹⁷ V. N. Zverev, M. Muhammad, S. Rahman, P. Debray, M. Saglam, J. Sigmund, and H. L. Hartnagel, *J. Appl. Phys.* **96**, 6353 (2004).
- ¹⁸ S. Datta and B. Das, *Appl. Phys. Lett.* **56**, 665 (1990).
- ¹⁹ E. N. Bulgakov and A. F. Sadreev, *Phys. Rev. B* **66**, 075331 (2002).
- ²⁰ S. M. Frolov, A. Venkatesan, W. Yu, J. A. Folk, and W. Wegscheider, *Phys. Rev. Lett.* **102**, 116802 (2009).
- ²¹ J. Wan, M. Cahay, P. Debray and R. Newrock, arXiv:0903.3915 (2009).